Abstract

The Oscillating Water Column (OWC) devices for wave energy extraction are equipped with Wells turbines for energy conversion. The effect of moisture in the air chamber of the OWC entails variations on the atmospheric conditions near the turbine, modifying its performance and efficiency. Through the theoretical development of a model for the facility, and the subsequent analysis of experimental tests carried out in a Wind Tunnel, we study in this work the influence of humid air in the performance of the turbine. Experimental analysis is carried out together with a real gas model to compare the observed behavior with the expected response.

1. Introduction

Wave energy extraction through *OWC* devices has been studied during the last decades. The study of this type of system has been analyzed on the basis of the analogy with oscillatory rigid bodies, as the OWC consists of a stationary chamber open at the bottom that allows the water surface inside to push the air above through the turbine [*Martins-Rivas and Mei (8)*].

Theoretical models have been tested in plants that are currently underway (*e.g.* Mutriku OWC in Basque Country, or Pico OWC in Azores). The main problem that arises is that the theoretical yields obtained do not match the reality [Mutriku OWC: Rated Power-300.000 kW; Real Power-300 kW *(11)*].

The operation of the OWC model has been developed by various authors. *Evans (4)*, *Evans and Porter (5)* formulated the problem of the oscillation of the water level in the chamber of OWC by linear wave theory. *Sarmento et al. (14)* extended the air expansion-compression problem inside the chamber. Finally, *Martins-Rivas and Mei (8)* reported a method of geometric control to maximize the efficiency of power extraction. All these authors consider an adiabatic process taking dry air as an ideal gas, but neither studied the mixture of dry air plus water vapour, nor makes any considerations regarding the nature of the real gas air.

In all previous references, the air compression and expansion are considered as isentropic processes of a perfect gas —an ideal gas with constant specific heat at constant volume. Consequently, the isentropic law is applied and linearized so the formulation is simplified. In fact, the reference conditions for the OWC are usually fixed as atmospheric, in which dry air is assumed and no further specifications on temperature, density or ambient moisture —dry air and water vapor mixture— are applied. In other words, no real gas model is taken into account. This is the motivation of our work.

Variations in the temperature, ambient

moisture and pressure are known to affect the turbine performance. Although the results are usually applied in different fields from that of sea waves energy extraction, the fundamentals of real gases could bring up a new scope in the real working conditions of OWC devices.

The influence of atmospheric conditions such as temperature and moisture on the performance of turbines has been widely considered, specially in problems related with gas turbines in power plants. The changes in performance arise from density diminishing, variations in the specific heat and gas constant, and for the eventual condensation of water vapor.

Referring to the study of air temperature effect, moisture and development of models of real gas in gas turbines, there is a lack of knowledge in the State of Art [see for details *Singh and Kumar (15)*, *Tsonopoulos and Heidman (17)*]. The first one *(15)*, analyzes the effect of ambient air temperature in the net power output on power plant performance. The second one *(17)*, uses the Virial Theorem to study real gas processes. Even if we establish the fundamental differences between OWC and gas turbine performances, a further step in the formulation of the OWC problem must be considered. We introduce a real gas in the model as well as the influence of ambient conditions, for which a full thermodynamic approach should be taken into account. To fulfill this task, we apply both the virial theorem or the Kammerling—Ones expansion [see *Tsonopoulos and Heidman (17)*].

Due to the limitations of the current models, it is desirable a gas model applied to the classical OWC development. This fact would help to understand the response of the OWC system and its relation with the principle of operation under real conditions. As a first approach, this paper studies the fundamentals of turbine operation under changes in density induced by variation of moisture content in steady state.

2. Background and objectives

2.1. Previous works in the research group

The works related to the OWC model started in 2006 with the *Cenit Project: Marine energies for desalination*. *Jalón et al. (6)* started the wave energy extraction studies. Afterwards, *Jalón Ramírez (7)* developed an optimization model of the OWC device.

Related to the OWC behaviour and the interaction between waves and structures, there are available several tests on the University of Granada Civil Engineering School wave basin, included in *Medina López (9)*. The main objective of those tests was the study of the radiation and diffraction phenomena, as well as the reflection problem and the resonance analysis of the cylindrical structure.

Focusing on the Wells turbine working, *Benslimane (1)*, *Benslimane (2)* developed a numerical model to analyse the influence of temperature and humidity, as well as an experimental study with dry air and low velocities ($u \leq 4m/s$).

2.2. Objectives

The main objective of this Masters Thesis is to study the effect of the working fluid density, mainly modified by humidity, on the performance of a Wells turbine on a steady state accounting for the real gas nature.

To reach this purpose, some specific aims have to be checked:

- To present the Wells turbine operating problem, considering it as a real gas model (mixture of dry air and water vapor).
- To experimentally verify the effect of moisture on the performance of a Wells turbine.
- To study a possible introduction of thermodynamic control in the turbine operation.

3. Methodology

To face these objectives, the methodology is essentially based upon experimental determination of pressure jump and flow characteristics in a simplified turbine model, and the theoretical formulation of the thermodynamic problem. The scheme shown in figure 1 describes the work flow to reach the final goals.

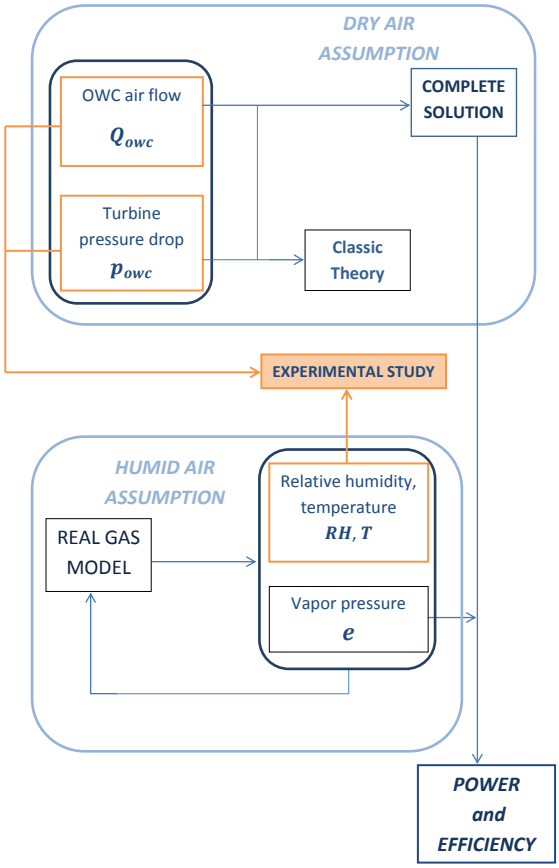

Figure 1: *General focusing on the research progress.*

4. Theoretical review

The main objective in this section is to replace the old *OWC* formulation for a new one, this last based on a real gas model, instead of the adiabatic process on an ideal gas. First of all, the classic problem will be analyzed. Afterwards, the real gas model will be introduced and applied to the theoretical model.

4.1. OWC model review. Classic formulation

In the classic problem, *Sarmento et al. (14)*, *Martins-Rivas and Mei (8)* measured the outer (thermodynamic) pressure in the chamber with a manometer, and they supposed that its value is constant. Nevertheless, they considered that the external pressure is time-dependent under operating conditions. For this reason, a new problem is presented, see the sketch depicted in figure 2, where P_0 and P_2 are the outer reference thermodynamic pressure and the thermodynamic total pressure inside the chamber of the OWC, respectively. The difference of these pressures is the the manometric pressure inside the chamber (p_{owc}) as it is stated in the following equation:

$$P_2 = p_{owc} + P_0\,. \tag{1}$$

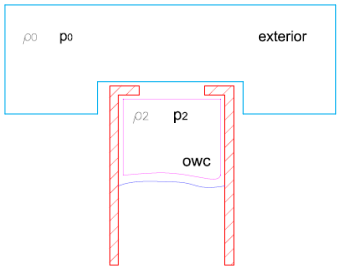

Figure 2: *Control volume scheme.*

The continuity equation applied to the control volume is:

$$\begin{aligned} Q_T^m &= -\frac{d}{dt}(\rho_2 V_{owc}) \\ &= -(\rho_2 \frac{dV_{owc}}{dt} + V_{owc}\frac{d\rho_2}{dt})\,, \end{aligned} \tag{2}$$

with the adiabatic relation,

$$pV^\gamma = constant\,, \tag{3}$$

and consequently

$$\frac{\rho}{\rho_{ref}} = [\frac{p}{p_{ref}}]^{1/\gamma}, \tag{4}$$

taking the solution (ρ_0,P_0) as a reference, the linear relations between pressure and density are established in equation (1):

$$\rho_2 = \rho_0 + \left(\frac{\rho_0}{\gamma P_0}\right)(p_{owc}). \tag{5}$$

The mass flow that go through the turbine, Q_T^m is defined respect to the external reference density as:

$$Q_T^m = \rho_0 Q_T = \rho_0 \frac{KD_T}{N\rho_0} p_{owc}, \tag{6}$$

where K depends on turbine parameters, following *(8)*, D_T is the turbine diameter and N is the turbine rotation velocity.

Substituting in equation (2), and multiplying by ρ_0, and Q_{owc} is cleared up:

$$Q_{owc} = \frac{KD_T}{N\rho_2} p_{owc} + \frac{V_{owc}}{C_s^2 \rho_2}\left(\frac{dp_{owc}}{dt}\right), \tag{7}$$

where C_s is the speed of sound in air.

Following *Martins-Rivas and Mei (8)* and applying harmonic solutions, we obtain:

$$\widehat{Q}_{owc} = \frac{KD_T}{N\rho_2}\widehat{p}_{owc} - i\omega\frac{V_{owc}}{C_s^2\rho_2}(\widehat{p}_{owc}), \tag{8}$$

where both $\widehat{Q}_{owc}$ and $\widehat{p}_{owc}$ are complex amplitudes defined in the classic problem.

In our work, we study a steady-state flow. Hence the continuity reads:

$$\boxed{Q_{owc} = \frac{KD_T}{N\rho_2} p_{owc}}, \tag{9}$$

with Q_{owc} and p_{owc} defined as real quantities.

In the classic problem, the air flow inside the *OWC* depends linearly on the pressure difference.

4.2. Pneumatic pressure and available power in the classic problem

Following *Martins-Rivas and Mei (8)*, the average power $\overline{W}$ is:

$$\begin{aligned}\overline{W} &= \frac{1}{2}\frac{KD_T}{N\rho_0}|\widehat{p}_{owc}|^2 \\ &= \frac{1}{2}\frac{KD_T}{N\rho_0}(\rho_w g)^2 \frac{|\tilde{\Gamma}'|^2 (H/2)^2}{(\chi+\tilde{B})^2 + (\tilde{C}+\beta)^2},\end{aligned} \tag{10}$$

and the capture length (understood as an efficiency expression) is:

$$\begin{aligned}kL &= \frac{8k\overline{W}}{\rho_w g H^2 C_g} \\ &= \frac{gkR_{owc}}{\omega C_g}\frac{\chi|\tilde{\Gamma}'|^2}{(\chi+\tilde{B})^2 + (\tilde{C}+\beta)^2}.\end{aligned} \tag{11}$$

Coefficients $\tilde{B}$, $\tilde{C}$, $tilde\Gamma$, χ and β are the mathematical representation of the oscillation damping and the restitution of the added mass, the flow in the chamber associated to the diffraction problem and the turbine characteristics. H is the wave height, C_g is the waves group celerity, $g = 9.81\, m/s^2$ is the gravity acceleration, k is the wave number and R_{owc} is the OWC radius.

4.3. Real gas properties

In the classic OWC problem, air is considered as a perfect gas bounded to a compression/exhaust adiabatic process inside the chamber and through the turbine.

A more complete description of the process consist of supposing that there exists a mix of dry air and water vapor inside the chamber, so the displaced fluid does not fit the ideal gas model. Some characteristics of the air–water vapor mixture are deduced from the properties of the vapor fraction. Using the *Clapeyron-Clausius* law *(16)* —figure 3—, the saturation vapor pressure e_s are defined as:

$$e_s = e_0 \cdot exp\left[\frac{L}{R_v}\left(\frac{1}{T_0} - \frac{1}{T}\right)\right], \tag{12}$$

where $e_0 = 0.611\,kPa$ is the partial saturation pressure at $T_0 = 273\,K$; L is the latent vaporisation heat; $R_v = 461\,J/K \cdot kg$ is the water vapor constant, and $L/R_v = 5423\,K$. The saturation pressure represents the equilibrium state for which no more vapor is present in dry air without further condensation, and it only deppends on temperature.

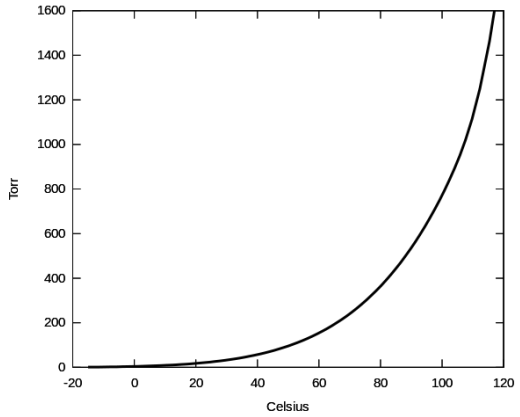

Figure 3: *Clapeyron-Clausius relation between saturated vapor pressure and air temperature. (10)*

However, the vapor pressure at any temperature —any non–equilibrium state— is determined from a given value of relative humidity (RH), expressed as the vapor concentration in dry air referred to the vapor concentration at equilibrium:

$$RH = \frac{e}{e_s}\,, \tag{13}$$

Therefore, the density of vapor present in the mix with dry air in the control volume, called absolute humidity, is:

$$\rho_v = \frac{e}{R_v T}\,, \tag{14}$$

The real gas density is corrected from the dry air density using the mixing ratio r, defined as the ratio between the masses of vapor and dry air

$$r = \frac{m_v}{m_a} = \frac{\epsilon e}{p}\,, \tag{15}$$

where $\epsilon = R_a/R_v = 286.7/461 = 0.622$. The moist air density is expressed as:

$$\rho_m = \frac{m_a + m_v}{V_m} = \frac{\rho_a V_a + \rho_v V_v}{V_a + V_v} = \frac{\frac{p}{R_a T} + \frac{p}{R_v T}}{V_a + V_v}\,, \tag{16}$$

where p and T are the pressure and temperature of the air-vapor mixture. This is deduced from the mixing ratio definition:

$$\frac{V_v}{V_a} = \frac{m_v R_v}{m_a R_a} = r\frac{R_v}{R_a} = \frac{r}{\epsilon}\,. \tag{17}$$

Finally, equation 16 is also expressed as:

$$\boxed{\rho_m = \rho_a \frac{1+r}{1+r/\epsilon} = \rho_a \frac{1+r}{1+1.608r}}\,. \tag{18}$$

4.3.1 Real gas model for the OWC

We start from the equation of state for N mols of an ideal gas:

$$pV = NR_0 T\,, \tag{19}$$

The real gas is expected to deviate from the ideal law, with the appearence of several interactions between different thermodynamic variables. To deal with the real gas, we start defining the compressibility factor per gas mole, $\mathbb{Z}$, *Biel Gayé (3)*, *Prausnitz et al. (12)*, as:

$$\mathbb{Z} = \frac{pV}{R_0 T}\,, \tag{20}$$

where R_0 is the universal gas constant. For an ideal gas, $\mathbb{Z} = 1$. A variation in the equation of state is carried out using the *Kammerling–Ones equation* (also known as the *Virial Expansion*) *Biel Gayé (3)*, *Prausnitz et al. (12)*:

$$\boxed{\mathbb{Z} = \frac{pV}{R_0 T} = 1 + \frac{\mathbb{B}}{V} + \frac{\mathbb{C}}{V^2} + \dots}\,, \tag{21}$$

where the second and third *virial* coefficients, $\mathbb{B}$ and $\mathbb{C}$, only depend on the temperature (experimental results).

An equation of state for a real gas is derived using $\mathbb{Z}$ defined in equation (21), *Yang and Su (18)*, *Tsonopoulos and Heidman (17)*:

$$p = \mathbb{Z}\rho_g R_g T\,, \tag{22}$$

where ρ_g and R_g are the real gas density and gas constant, determined from equation (16). Therefore the compressibility factor $\mathbb{Z}$ is expressed from equation (21) in the alternative form proposed by *Tsonopoulos and Heidman (17)*, with truncated series up to the second virial coefficient:

$$\mathbb{Z} = 1 + \frac{\mathbb{B}p_c}{R_g T_c}\frac{p_r}{T_r}. \tag{23}$$

In the previous expression p_c and T_c are the critical values of pressure and temperature for a given gas. Critical temperature and its corresponding pressure value represent the state beyond which a gas cannot be liquified by compression, and they are standard reference values used for calculations with reduced state variables T_r and p_r, so that $T_r = T/T_c$ and $p_r = p/p_c$. In the case of water $T_c = 647\,K$ and $p_c = 218\,atm = 220.89 \cdot 10^5\,Pa$. The advantage in the previous formulation is that equation (16) is therefore calculated from, *Tsonopoulos and Heidman (17)*:

$$\frac{\mathbb{B}p_c}{R_g T_c}\frac{p}{T} = f_0 + \omega f_1 + \chi_{mol} f_2\,, \tag{24}$$

where: f_1, f_2 and f_3 are temperature correlation functions; ω is the acentric factor; χ_{mol} is the molar fraction of vapor in dry air. In the case of the air-water vapor mixture —hereinafter the real gas—:

$$\begin{cases} \omega \simeq 0 \\ f_0 = 0.145 - \dfrac{0.33}{T_r} - \dfrac{0.1385}{T_r^2} - \dfrac{0.0121}{T_r^3} - \dfrac{0.000607}{T_r^8} \\ f_2 = \dfrac{0.0297}{T_r^6} - \dfrac{0.0229}{T_r^8}. \end{cases} \tag{25}$$

Once the virial terms and compressibility factor are determined, is straightforward to estimate the specific heat and the enthalpy for the real gas, as deviations from the ideal gas values, *Yang and Su (18)*:

$$C_{p\,g} = C_p + \delta C_p p\,, \tag{26}$$

and:

$$H_g = H + \delta H p\,, \tag{27}$$

where the deviations of specific heat and enthalpy are:

$$\delta Cp = -\frac{R_g T_r}{p_c}\frac{d^2}{dT_r^2}\left(f_0 + \chi_m f_2\right)\,, \tag{28}$$

and:

$$\delta H = \frac{R_g T_c}{p_c}\left(f_0 + \chi_m f_2\right) - T_r \frac{d}{dT_r}\left(f_0 + \chi_m f_2\right)\,. \tag{29}$$

Following the methodology proposed by *Yang and Su (18)* in a simplified way and making use of equations (26) to (29), the conservation of enthalpy is applied between turbine inlet and outlet, with known values of local temperature, pressure and humidity at the inlet. Recalling that the enthalpy for the ideal gas is expressed as:

$$H = C_p T + \frac{1}{2}U^2\,, \tag{30}$$

the velocity at the turbine outlet is computed from equations (27) and (30) for the real gas:

$$U_{out} = \left(2(H_g - C_p T_{out} - \delta H p_{out})\right)^{0.5}\,, \tag{31}$$

Here the temperature T_{out} should not be evaluated through the adiabatic process equation $T_{out}^{ad} = T_{in}(p_{out}/p_{in})^{(\gamma-1/\gamma)}$, because strictly speaking this last expression is only valid for ideal gas. Instead of using this last equation, a new value of $T_{out} \neq T_{out}^{ad}$ is supposed until the continuity condition is satisfied:

$$\rho_g US\big|_{in} = \rho_g US\big|_{out}\,. \tag{32}$$

The iterative procedure, in which the effect of moisture is implemented through the

density and the real gas constant R_g, outcomes new pressure and temperature values for the real gas. Applying this methodology, we will observe differences between the ideal and real gas models.

4.4. Turbine dynamics

The OWC uses a power take off system for transformation of pneumatic energy into electricity to be supplied to the grid. Usually, it uses a turbine to accomplish with that purpose.

The primary input for the design of a turbine is the pneumatic power based upon the pressure amplitude (P) and the volume flow rate Q at turbine inlet. The performance indicators are the pressure drop, power and efficiency, and their variation with the flow rate. The aerodynamic design and consequent performance is a function of several variables that have been listed by *Raghunathan (13)*.

In general terms, the turbine performance is described by the following non-dimensional coefficients:

- Flow coefficient:

$$\Phi = \frac{V_x}{U}\,, \tag{33}$$

- Pressure drop:

$$P^* = \frac{\Delta P}{\rho_2 w^2 D_t^2}\,, \tag{34}$$

- Solidity:

$$\sigma = \frac{A_a}{\pi(D_t/2)^2}\,, \tag{35}$$

  where V_x is the axial velocity, $U = ND_t/2$ is the blade circumferential velocity, w is the relative incoming velocity, A_a is the whole blades area. $F_x = \Delta P A_a$.

The power input is expressed as:

$$\boxed{W_I = \Delta P Q}\,. \tag{36}$$

To maximize the power input, it is necessary to deal with the pressure jump.

5. Experimental set up

We describe in this section the methodology used to conduct tests in a wind tunnel. The turbine performance has been tested with a total of three different environmental conditions: so called "dry air" (non forced humidity, environmental conditions, $\approx$ 35% relative humidity), humid air with minimum humidity (50% relative humidity) and humid air with maximum humidity (70% relative humidity).

5.1. Wind tunnel

The wind tunnel is a poly-methylmethacrylate (*PMMA*) structure with a test section that is $3\,m$ in length with a $360\,mm \times 430\,mm$ cross-section. The wind speed, up to $20\,m/s$, is controlled by a variable frequency converter controlling an electric fan at the downstream end with a maximum power of $2.2\,kW$.

First of all, the wind tunnel calibration was made. This tunnel is controlled by an inverter *Siemens Micromaster 420*. An input voltage is introduced to the inverter, and this transforms it to a valid voltage for the wind tunnel engine. With the calibration, it is desirable to know the relation between input voltage and wind velocity.

The calibration has been made in dry tests, so the measure is not affected by humidity. The measure was done with a *Prandtl tube*. This takes total (P_T) and static (P_s) pressure data, and with these, it is calculated the velocity as:

$$v = \sqrt{\frac{2(P_T - P_s)}{\rho}}\,, \tag{37}$$

where ρ is the fluid density.

The calibration curve obtained is depicted in figure 4, finding a linear response with the input voltage, with a linear regression coefficient $R = 0.9979$. The maximum input voltage, $10\,V$, is equivalent to a wind velocity of $11.7 m/s$ for the used configuration in the inverter.

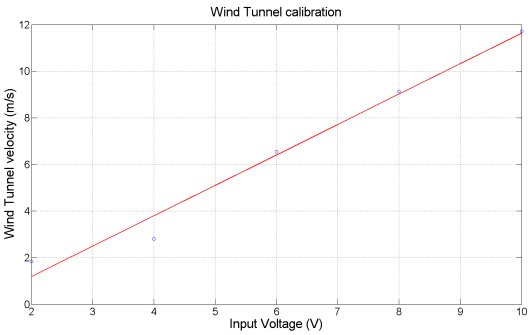

Figure 4: *Wind Tunnel calibration.*

5.2. Turbine

It has been used a turbine of diameter $D_t = 0.025\,m$. The turbine frontal area is $A_t = 3.5906 \cdot 10^{-4}\,m^2$, and the turbine blades area is $A_a = 2.4271 \cdot 10^{-4}\,m^2$. The turbine solidity, required for equation (35), has a constant value of $\sigma = 0.3434$.

Figure 5: *Image of the turbine and the nylon structure.*

This turbine, shown in figure 5, has been assembled on a nylon structure which simulates an *OWC* (see figure 5).

5.2.1 Turbine calibration

The rotation velocity of the used turbine was calibrated. As shown in figure 6, the relation between rotation speed and wind tunnel air velocity is linear until the turbine reaches its terminal velocity.

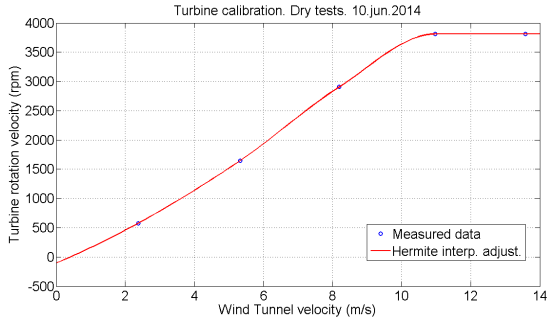

Figure 6: *Turbine calibration.*

5.2.2 Experimental model scope and restrictions

The turbine is not a Wells turbine strictly speaking, so the one used in this study does not rotates in the same direction independently of the air flow, as the real Wells turbine does.

These two turbines have the same behaviour, as the relation between air flow and pressure is linear, see figure 7.

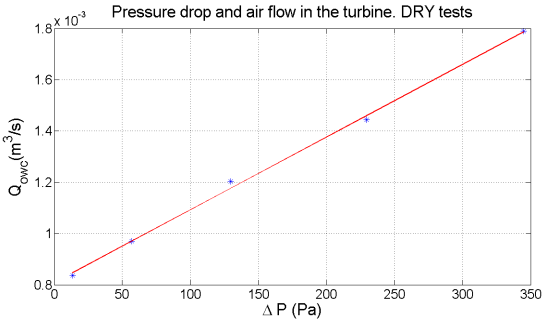

Figure 7: *Air flow and pressure drop in turbine.*

This fact allows focusing on the humidity change and its effect in flow and turbine rotation. Additionally, in these tests there is an important fact to be considered: the forced environmental conditions inside wind tunnel (humidity and temperature) are unique. The repeatability of the experiments is almost null, as the moist measurement depends on a high number of other factors: external temperature, time of the day, season and wind tunnel location. There is a high level of humidity in the laboratory, so it is a really influencing condition on wind tunnel moisture.

5.3. Water spray gun

A paint spray gun is used with water to seed the wind tunnel with small water particles.

The gun is situated in front of the wind tunnel entrance, so the engine in the other end of the tunnel sucks the air and water particles out, generating and humid air circulation.

The nozzle aperture is controlled with a faucet in the bottom of the gun. In the measurements presented in this work, the maximum and the minimum apertures have been tested to allow us maximum and minimum humidity conditions inside the tunnel, respectively.

5.4. Measurement instruments

5.4.1 Pressure

The pressure measurements have been conducted with the pressure system *DTC Initium* by *Measurement Specialties INC*. It consists of a number of pressure taps (up to 64 channels per scanner). These work at a sampling period of $0.0016\,s$. Six pressure taps have been located around the turbine: two of them in the flow direction to measure total pressure, and the rest four samples perpendicular to the flow direction, for the static pressure measurement (see figure 8). There are two static pressure taps and two total pressure taps place upstream the turbine, and two static pressure taps placed downstream.

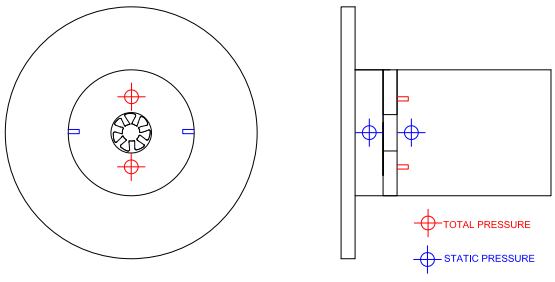

Figure 8: *Pressure taps distribution.*

5.4.2 Air flow velocity

The wind velocity has been measured with a *Laser Doppler Velocimeter (LDV)* by *TSI*. This is a extremely precise technique, and as a seeding, it is used the water particles in the wind tunnel. Hence it is obtained a complete velocity profile in every point needed. In this case, it has been measured the velocity upstream and downstream turbine.

5.4.3 Turbine rotation

The turbine rotation has been measured with a Laser Distance Measurement Device *Selcom SLS5000*. The main objective of this device is measuring distances. Thus, every time a blade passes through the laser, its signal changes. Obviously, if the blade remains at the same distance, the laser gives an identical signal for every single blade of the turbine. With an spectral analysis of the signal, the average rotation frequency is obtained.

5.4.4 Humidity and temperature

The measurement of humidity and temperature has been done with a weather station *Oregon Scientific BAR908HG*. This can support a maximum of five thermo-hygrometer remote sensors.

In this case, it have been used three remote sensors, using in addition the sensor inside the station to measure the external temperature and humidity.

The three remote sensors were located at three representative sections inside the wind tunnel (*S1*, *S2* and *S3*), as shown in figure 11. The first one is placed near the entrance to control the input humidity. The second one is situated upstream the turbine, near it, and the third one, downstream.

At first instance, some equilibrium humidity tests were performed to analyse how humidity changes with time. In the final tests and in order to obtain accurate results, it was required experimentally to have a humidity level as constant as possible.

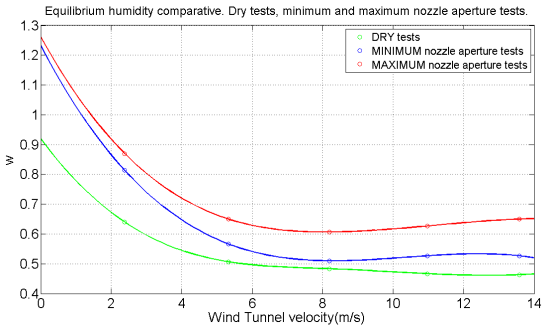

Figure 9: *Equilibrium humidity.*

The humidity takes higher values for lower wind velocities. As the velocity grows, the humidity decreases until a point in which it remains constant. This effect takes place when the thermodynamic equilibrium is reached inside the wind tunnel.

The final set up, with the thermo-hygrometer sensors and the LDV measurement points is shown in figure 11.

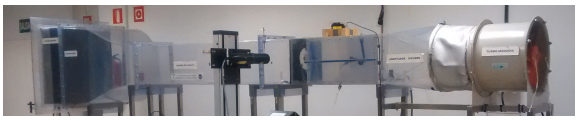

Figure 10: *Wind Tunnel.*

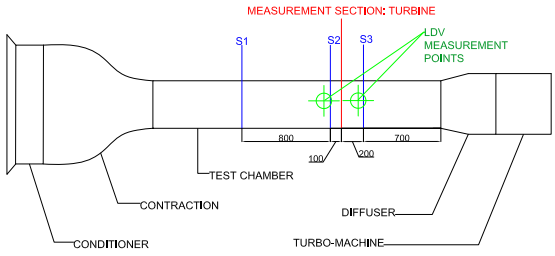

Figure 11: *Final set up.*

6. Results and discussion

In this section, experimental results are presented alongside the theoretical prediction through the real gas model shown in previous sections.

6.1. Turbine rotation

The linear relation between turbine rotation velocity and wind tunnel velocity was shown in figure 6. Now, a comparative between rotation velocity in two different humidity conditions is presented.

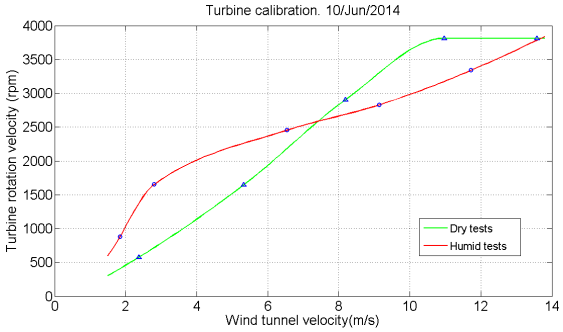

Figure 12: *Turbine calibration. Different humidities.*

For dry tests (non forced ambient humidity), the rotation velocity function is linear versus the wind velocity, up to the value of $11\,m/s$ where the turbine reaches its terminal velocity.

For the humid tests, the relation between rotation and wind velocity is not anymore linear. In fact two inflections points are shown in figure 12 for wind tunnel velocities of $4\,m/s$ and $10\,m/s$, approximately. Moreover, humid tests are above the dry ones for wind velocities lower than a critical wind tunnel velocity, $V_c = 7.5\,m/s$ (average of the two inflection points). It implies that, for lower velocities than V_c, the turbine runs faster with high values of humidity. On the other hand, the turbine rotates slower than under dry conditions for greater values of the velocity inside the wind tunnel than V_c. Therefore, the humidity has a strong influence on the operating conditions of the turbine. Finally, it is worth mentioning that the rotation-rate does not achieve the terminal velocity under humidity conditions.

6.2. Upstream velocity profile

In the experimental set up, the OWC nylon structure pit is an obstacle to the air flow, enhancing the formation of stagnation points in the edges of the structure. To quantify this

aspect, some velocity measurements have been carried out by using *LDV* in the inlet region of the structure.

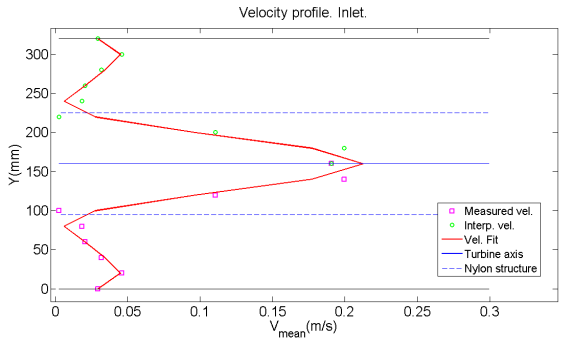

Figure 13: *Velocity profile. LDV.*

The velocity profile grows around the turbine orifice, with a minimum in the itersection with the nylon structure. The values are lower than in the downstream because of the energy conservation: a decrease in pressure implies an increase in velocity.

6.3. Pressure drop and air flow

The pressure difference between upstream and downstream was measured for every test.

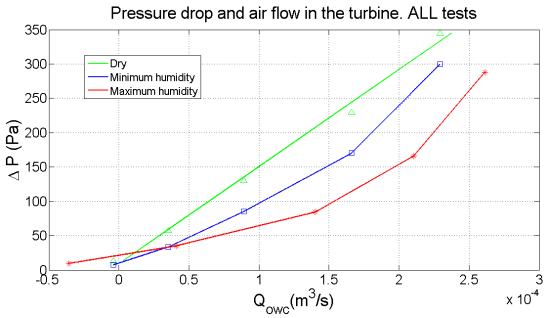

Figure 14: *Pressure drop and air flow.*

It is shown in figure 14 that the pressure—flow rate curves for humid air present a different behaviour in comparison to the dry air one. In addition, as humidity increases, the curve moves away from the dry air one. In other words, it is neccessary greater flow rates to obtain the same pressure drop as humidity increases. Consequently, humid air brings less power to the turbine, as shown in following sections.

6.3.1 Non-dimensional pressure drop and air flow

As presented in equations (33) and (34), in the classic turbines literature, the turbine performance is described by some non-dimensional coefficients. In our case, a representation of the pressure drop and the air flow in terms of non-dimensional coefficients is useful for later comparison with future tests.

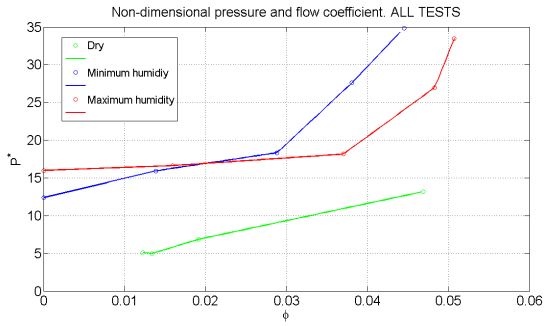

Figure 15: *Non-dimensional pressure drop and air flow.*

The results are depicted in figure 15. Dry air curve exists in a different non-dimmensional pressure range than the humidity cases. For $\phi \geq 0.02$, when the flow starts to be significant, and non–linear effects are neglected, the curves with humidity start to diverge with respect to the air flow.

The behavior of dry air curve with respect to the other two humidity curves is different. For the two humidity curves, the pressure range is the same. As well as in the dimensional case, with greater humidity, to obtain the same pressure a higher flow coefficient is necessary.

6.4. Density correction by the air–vapor mixture

We have seen in previous sections that the form of the curves ΔP–Q is different deppending on the humidity content of the air flow. A first attempt in predicting the turbine response under moist air condition, is performed by

substituting moist air densities calculated by equation (18) in the classic continuity equation (9). But in this case, the classic formulation does not allow to predict successfully the turbine response under moist condition, as depicted in figure 16.

The turbine response for dry conditions is fairly well predicted with the classic formulation. However, the moist conditions do not match the experimental results. That way, the classic continuity expression might result incomplete for the prediction of the turbine performance with humid air, even if the actual turbine also offers a linear response in dry air.

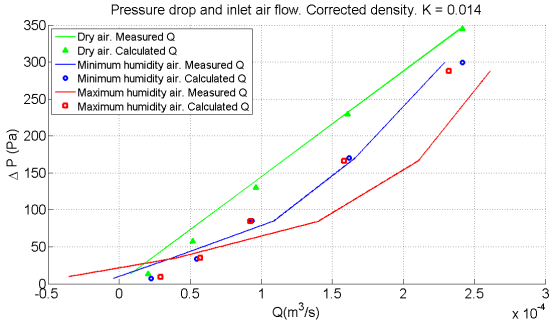

Figure 16: *New humidity curves. Corrected density.*

6.5. Temperature calculations for the real gas model and compressibility factor $\mathbb{Z}$

Following the methodology proposed for the real gas, values of temperature at the turbine outlet are predicted for the experimental turbine inlet data. Temperature calculations are carried out under conservation of enthalpy and mass flow. As a result, there are observed differences with respect to the calculated values under the asumption of adiabatic process for an ideal gas, as it is shown in figure 17.

The plots present the same behavior in all cases. For the lower moisture content, the real gas model shows a constant temperature value for the complete range of pressure, while the differences become more significant as humidity increases. The differences can be explained from the standpoint of the real gas. The adiabatic law, $pV^{\gamma} = constant$, is suitable for an ideal gas, say, a gas addressing the thermal equation of state $p = \rho RT$ for all T. But according to the above dissertation, in a real gas we have $p = Z\rho RT$ which means that ρRT is not always followed exactly; then the adiabatic law in its standard form might not be fully applicable.

However, the previous results are not incompatible with the hypothesis of adiabatic process. Actually, the adiabatic law $pV^{\gamma} = constant$ is deduced from three fundamental hypothesis, *Biel Gayé (3)*: (1) ideal gas equation of state $p = \rho RT$; (2) First Principle of Thermodynamics applied to a thermally isolated system, which means no heat exchange with the exterior; (3) the work exerted on the system takes the form of a reversible process under constant pressure condition. In the case of an air–water vapor mixture, the hypothesis of thermal isolation and reversible process are applicable as in other local atmospheric processes. But the presence of vapor in air and the subsequent induced changes as a funtion of temperature —mixture density, saturation pressure, etc. — induce a deviation from the ideal gas law. In fact, it is assumed that the flow through the turbine is adiabatic, but with a new law different from the ideal one.

This can be further observed in the calculations of the compressibility factor $\mathbb{Z}$.

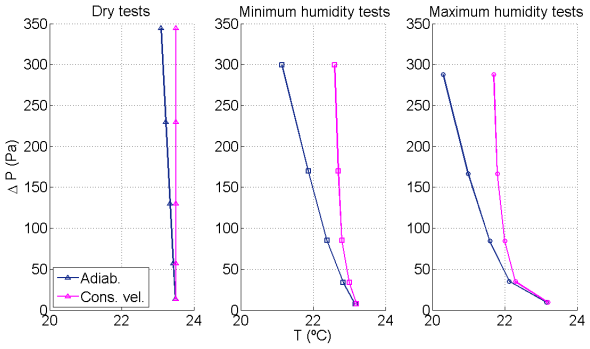

Figure 17: *Pressure drop and different temperatures.*

The compressibility factor $\mathbb{Z}$ is calculated

following equation (23) and plotted in figure 18 for the case study. The compressibility factor gives information about the deviation of the real gas behavior from the expected ideal response. The behavior of $\mathbb{Z}$ is linear for the whole range studied, i. e. between 22.6 °C and 23.2 °C, with overlapping of minimum and maximum humidity curves. The values keep away from 1 (that value would be equivalent to an ideal gas) as temperature decreases.

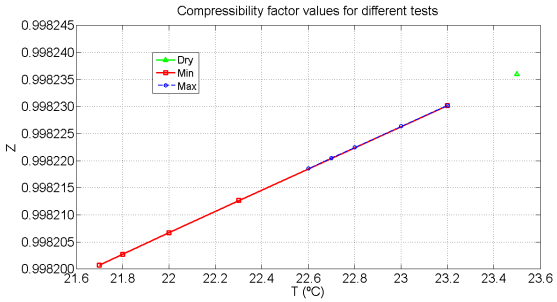

Figure 18: *Compressibility factor $\mathbb{Z}$. Different tests.*

However, the linear trend in $\mathbb{Z}$ is only preserved for low temperature values, as shown in figure 19, while for high temperatures —say for reduced temperatures $T_r \gtrsim 0.7$— tends to an asymptote $\mathbb{Z} \to 1$, accordingly to the real gas model.

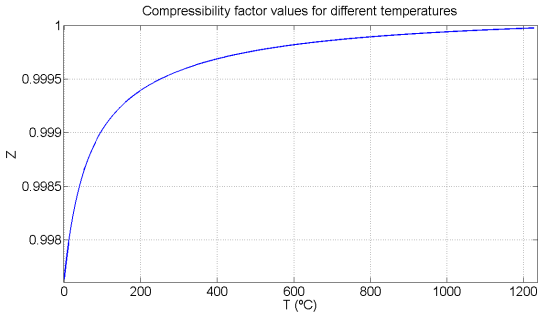

Figure 19: *Compressibility factor $\mathbb{Z}$.*

As temperature decreases the gas behavior differs from the ideal one. This result is consistent with others obtained: humidity in air makes this gas different from an ideal gas.

6.6. Power input

Power input is calculated as shown in equation (36). The results obtained are presented in figure 20.

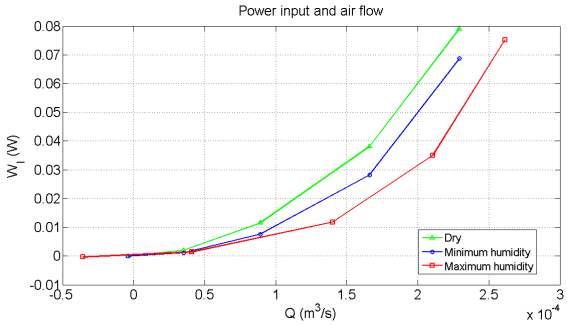

Figure 20: *Power input and air flow.*

Following the same argument of previous results, the power input decreases as humidity increases, for a constant flow rate. In other words, to obtain the same power input it is neccesary greater flow rates with greater values of humidity.

7. Conclusions

Throughout the development of this work it has been shown the behavior of moist air on the operation of an air turbine. In particular, the results presented after the application of the theoretical model of real gas are intended to be further applied to improve the performance of OWC devices.

The relation between pressure drop and air flow in classic theory is linear, and the hypothesis of dry air and ideal gas are assumed. With these experimental tests it has been observed that this relation is not linear with moist air. Furthermore, it has been justified for the air–water vapor mixture, that linear curve decreases towards the experimentally observed values when moisture exists.

It has been found that the flow through the turbine does not address the ideal gas law, hence the adiabatic equation for the ideal gas is not fully applicable. For the conservation of mass flow and enthalpy to be fullfilled, a real

gas model has to be applied. In that sense, it has been verified that the real gas temperature output differs from the ideal gas adiabatic prediction. Moreover, as humidity increases the difference between adiabatic temperature and flow conservation temperature grows.

The compressibility factor is close to 1, but does not take exactly that value. The real gas differs slightly from the ideal model. The state equation for the real gas differs from the ideal case, and therefore its behavior keeps away from the ideal adiabatic description of the process.

It has been found that power input decreases when moisture increases. The difference between expected power output values and real power obtained in operating OWC plants may be revised under these considerations.

7.1. Future research

As future research lines, the following are posed:

- To study experimentally the influence of harmonic solutions on the turbine performance together with humidity.
- To introduce a thermodynamic control of the turbine to optimize the OWC performance, using the presented results.
- To reformulate the classic OWC theory including moisture effects and a new adiabatic equation for the real gas.

Appendix: Air properties

	Property	*Units*
R_a	286.7	$J/kg \cdot K$
C_p	1010	$J/kg \cdot K$
ρ_a	1.25	kg/m^3
MW_a	0.0288	$kg/mole$
R_v	461	$J/kg \cdot K$
T_{cv}	374.4	$^\circ C$
p_{cv}	$220.89 \cdot 105$	Pa
MW_v	0.0182	$kg/mole$

Table 1: *Dry air and vapor properties.*

References

[1] S. Benslimane. Experimental study of the effect of blade sweep on the performance of wells turbine. Technical report, University of Granada., 2013.

[2] S. Benslimane. Test wells turbine. Technical report, University of Granada., 2014.

[3] J. Biel Gayé. *Formalismo y método de la termodinámica. Teoría general, aplicaciones y ejercicios resueltos. Apuntes de clase.* Universidad de Granada, 1986.

[4] D. Evans. Wave-power absorption by systems of oscillating surface pressure distributions. *Journal of Fluid Mechanics*, (114):481–499, 1982.

[5] D. Evans and R. Porter. Hydrodynamic characteristics of an oscillating water column device. *Applied Ocean Research*, (17):155–164, 1995.

[6] L. Jalón, A. Moñino, A. Baquerizo, and M. Losada. Proyecto cenit tecoagua. informes técnicos., 2006.

[7] M. Jalón Ramírez. Probabilibdad de fallo de un dispositivo de aprovechamiento de la energía undimotriz frente acción del oleaje. Master's thesis, Máster en Ingeniería de estructuras. E.T.S. Ingeniería de Caminos, CC. y PP. Universidad de Granada., 2008.

[8] H. Martins-Rivas and C. Mei. Wave power extraction from an oscillating water column at the tip of a breakwater. *J. Fluid Mechanics*, (626):395–414, 2009.

[9] E. Medina López. Estudio de la interacción oleaje-estructura. Aplicación a estructura cilíndrica para dispositivo undimotriz. Technical report, Final Degree Project. Universidad de Granada, 2013.

[10] NASA. http://www.nasa.gov, 2014.

[11] Power-technology. http://www.power-technology.com/projects/mutriku-wave/, 2014.

[12] J. Prausnitz, R. Lichtenthaler, and E. G. de Azevedo. *Molecular Thermo-Dynamics of Fluid–Phase Equilibria.* Prentice–Hall, 1999.

[13] S. Raghunathan. The wells air turbine for wave energy conversion. *Prog. Aerospace Sci.*, (31):335–386, 1995.

[14] A. Sarmento, L. Gato, and A. Falcao. Turbine-controlled wave energy absorption by oscillating water column devices. *Ocean Engineering*, 17(5):481–497, Jan. 1990.

[15] S. Singh and R. Kumar. Ambient air temperature effect on power plant performance. *International Journal of Engineering Science and Technology (IJEST)*, 4(8):3916–3923, 2012.

[16] R. B. Stull. *Meteorology for scientists and engineers.* Pacific Grove, CA, 2000.

[17] C. Tsonopoulos and J. Heidman. From the virial to the cubic equation of state. *Fluid Phase Equilibria*, (57):261–276, 1990.

[18] W. Yang and M. Su. Influence of moist combustion gas on performance of a sub-critical turbine. *Energy Conversion & Management*, (46):821–832, 2004.